PHYSICAL REVIEW D **76,** 083522 (2007)

Dark matter and Higgs boson physics

Francesco D'Eramo
Scuola Normale Superiore, Piazza dei Cavalieri 7, I-56126 Pisa, Italy
(Received 26 July 2007; published 25 October 2007)

A vectorlike colorless fermion doublet and a singlet added to the standard model allow a consistent interpretation of dark matter in terms of the lightest neutral particle, as they may help in obtaining successful gauge coupling unification. We analyze in detail the mass range of the lightest neutral particle below the W mass, i.e. in a range of the parameters where the physics of the standard model Higgs boson may be substantially affected either directly or indirectly.

DOI: 10.1103/PhysRevD.76.083522 PACS numbers: 95.35.+d, 14.80.Bn, 98.80.Cq

I. INTRODUCTION

The standard model (SM) of the electroweak interactions is more than 30 years old and it has been able to reproduce with great precision the many experimental results obtained until now. In particular, at the CERN LEP the theory was tested at the per mille level without finding any discrepancy with the theoretical predictions. However, in spite of this extraordinary success, we are convinced of new physics beyond the SM, since there are problems where the SM does not provide an adequate solution. One of these, supported by observations, is the lack of a dark matter candidate.

The most direct and impressive evidences of the existence of dark matter are surely the flat rotation curves of spiral galaxies. Other evidences for dark matter were found at different scales, from galactic scales (several kiloparsecs) and clusters of galaxies (Megaparsecs) to global scales of hundreds of Megaparsecs [1]. The total matter density can be inferred from the measurements of the power spectrum of the fluctuations in the cosmic microwave background (CMB). The recent measurements of the Wilkinson Microwave Anisotropy Probe (WMAP) [2] have shown that the total matter abundance in the universe is $\Omega_m h^2 = 0.1277^{+0.0080}_{-0.0079}$; these measurements have also provided the baryon abundance which is $\Omega_b h^2 = 0.022\,29 \pm 0.000\,73$. We conclude that all the matter in the universe cannot be baryonic and that the dark matter abundance is $\Omega_{\mathrm{DM}} h^2 = 0.1054^{+0.0080}_{-0.0079}$. The fact that a significant part of dark matter must be nonbaryonic was known before WMAP measurements. Indeed an estimate of $\Omega_m h^2$ was already available [3], and the value of $\Omega_b h^2$ was inferred from primordial nucleosynthesis [4]; the difference seemed notable also at that time. Additional evidence for the nonbaryonic nature of dark matter is given by structure formations: in a universe with only baryons the primordial density perturbations have not had enough time to grow and generate the galaxies observed today in the sky. These observations, however, do not tell us anything about the particle nature of dark matter. Then the question is about the nature, the origin, and the composition of this important component of our universe, since dark matter does not find an explanation in the framework of the standard model of particle physics.

Particle physics provides us with a large number of dark matter candidates, which appear naturally in various frameworks for reasons completely independent from the dark matter problem, and certainly not invented for the sole purpose of explaining the presence of dark matter in our universe. Among these candidates an important distinction is between particles created thermally or not thermally in the early universe. For thermal relics another important distinction is how they decoupled from the primordial soup, in particular, if they were relativistic (hot dark matter) or nonrelativistic (cold dark matter). Arguments from large structures make us believe that a large, and presumably dominant, fraction of dark matter is made of cold relics. A well-motivated class of cold dark matter particles are the so-called weakly interacting massive particles (WIMPs), which have mass between 10 GeV and a few TeV and interact only through weak and gravitational interactions, because the limits on charged relics are very stringent [5].

Another missing opportunity for the standard model is that gauge couplings do not quite unify at high energy; a possible solution is to add weakly interacting particles to change the running, in order to make unification work better.

In this work we discuss a model that has both a cold dark matter candidate and can improve considerably over the standard model in the direction of successful gauge coupling unification. We introduce new matter with respect to the standard model alone, and we restrict ourselves to the case in which the added particles are fermions. Adding just a vector doublet allows remarkable improvements for unification; this model, furthermore, is highly constrained since it contains only one new parameter, the Dirac mass for the degenerate doublets, whose neutral components are the dark matter candidates. Such a model, however, is ruled out by direct detection experiments: the vectorlike vertex with the Z boson for the neutral particles remains unsuppressed, giving a spin-independent cross section that is 2–3 orders of magnitude above current limits [6]. This drawback can be solved by including a fermion singlet, with

Yukawa couplings with the doublets and the Higgs boson. Doing this, we generate a mixing between doublets and a singlet, so that the neutral particles become Majorana fermions which have suppressed vectorlike couplings with the Z boson. We assume a parity symmetry that acts only on the new fields. This imposes that they do not couple to ordinary matter. It also implies that the lightest particle is stable and, if neutral, it constitutes a good dark matter candidate. This model has been introduced in Ref. [7] where a detailed dark matter analysis for high values of the relic particle mass can be found. In Ref. [7] it is also shown how the gauge coupling unification at high energy can be achieved, and a rate for the proton decay is predicted that could be tested in the future.

In this work we focus on the region of parameter space where the mass of the lightest neutral particle (LNP) is smaller than the W boson mass $m_W \approx 80$ GeV. The analysis for higher mass was already done, as said above, but the main reason for doing so is that well above the WW production threshold, in order to account for the entire dark matter abundance observed, the mass M of charged components of the doublets is quite high. An important fact is that, for relatively low values of the LNP mass, the effects on Higgs boson physics are significant, both direct and indirect. On the one hand, there are newly available decay channels for the Higgs boson, and the decays into neutral particles may dominate the total width. On the other hand, the new particles contribute to electroweak observables, so that they may change the indirect upper limit on the Higgs mass and improve the naturalness of the Higgs potential [8]. There are thus reasons to give special attention to this region of parameter space.

The structure of this paper is as follows: in Sec. II we present the model with its spectrum, in Sec. III we compute the relic abundance of the dark matter candidate, in Sec. IV we discuss direct detection, and in Sec. V we discuss the effects on Higgs boson physics. Finally, in Sec. VI we consider a possible CP violating phase giving rise to an electron electric dipole moment (EDM). Conclusions are given in Sec. VII.

II. THE MODEL

The model consists of the following extension of the standard model:

$$\mathcal{L} = \mathcal{L}_{\rm SM} + \Delta\mathcal{L} \tag{1}$$

where we add to the standard model Lagrangian the following renormalizable Lagrangian (other than the kinetic terms for the various new fields):

$$\Delta\mathcal{L} = \lambda F H S + \lambda^c F_c H^\dagger S + M F F_c + \mu S^2 + \text{H.c.} \tag{2}$$

The doublets F_c and F have, respectively, hypercharge $\pm 1/2$, S is a singlet, and H is the standard model Higgs doublet. We introduce the symmetry

$$F, F_c, S \rightarrow -F, -F_c, -S \tag{3}$$

with all other fields invariant. This imposes that the new fields do not couple to ordinary matter. We suppose the parameters $(\lambda, \lambda^c, M, \mu)$ to be real (in Sec. VI we will consider the effects of introducing a phase). The physical fields are chosen as follows:

$$F_c = \begin{pmatrix} F^+ \\ F_c^0 \end{pmatrix}, \qquad F = \begin{pmatrix} F^0 \\ F^- \end{pmatrix}, \qquad H = \begin{pmatrix} \phi^+ \\ v + \frac{h + i\chi}{\sqrt{2}} \end{pmatrix}. \tag{4}$$

The components of F_c and F are left-handed Weyl fields. The Goldstones ϕ^+ and χ can be put to zero by choosing the unitary gauge.

In the charged sector there is a simple Dirac term of mass M; hence we define the Dirac spinor $\psi = F_c^+ + (F^-)^c$.

In the neutral sector we define the fields N_i as

$$N_1 = \frac{1}{\sqrt{2}}(F_c^0 - F^0), \qquad N_2 = \frac{1}{\sqrt{2}}(F_c^0 + F^0), \qquad N_3 = S, \tag{5}$$

so that the mass matrix takes the form

$$M_N = \begin{pmatrix} M & 0 & -\sqrt{2}\beta v \\ 0 & -M & -\sqrt{2}\alpha v \\ -\sqrt{2}\beta v & -\sqrt{2}\alpha v & -2\mu \end{pmatrix} \tag{6}$$

where the Yukawa couplings have been replaced by the parameters

$$\alpha = \frac{\lambda^c + \lambda}{2}, \qquad \beta = \frac{\lambda^c - \lambda}{2}. \tag{7}$$

We now have to find eigenvalues and eigenvectors of this matrix; in the general case this task cannot be accomplished analytically and therefore we will diagonalize the mass matrix numerically. Let m_i be the eigenvalues and let V be the matrix that performs the diagonalization. We define χ_i as the eigenvector corresponding to m_i, i.e.

$$N_i = V_{ij}\chi_j, \qquad V^t M_N V = \text{diag}(m_1, m_2, m_3). \tag{8}$$

We identify the lightest neutral particle (LNP) with the index l; then χ_l is the field of the LNP.[1]

III. DARK MATTER ANALYSIS

In this section we compute the thermal relic abundance of the LNP using the standard formalism [9]. Before proceeding, we should justify why we can use it, because there are situations in which this method fails [10]. We have checked that, in the parameter region of interest to us, the masses of the other two neutral and of the charged

[1]From now on, the index l for χ_l indicates *lightest*, and it must not be confused with *left*.

particles are far higher than the LNP mass itself, so we can neglect coannihilations. The standard method is also not valid when the relic particle lies near a mass threshold since the LNP particles are Boltzmann distributed. Given our LNP mass range the only threshold present is that for WW production. For $m_l \geq 75$ GeV the WW process suppresses the LNP relic abundance to an unacceptable level, whereas for $m_l < 75$ GeV it can be safely neglected.

The evolution of the LNP number density n_l is governed by the Boltzmann equation

$$\frac{dn_l}{dt} + 3Hn_l = -\langle \sigma v_{\rm rel} \rangle [n_l^2 - (n_l^{\rm eq})^2] \tag{9}$$

where H is the Hubble parameter, $n_l^{\rm eq}$ is the LNP equilibrium number density, $v_{\rm rel}$ is the relative velocity, and $\langle \sigma v_{\rm rel} \rangle$ is the thermal average of the annihilation cross section. The relevant temperatures are of order $m_l/25$, so the Boltzmann equilibrium distribution is well justified. The Boltzmann equation can be solved approximately. First we introduce the variable $x \equiv m_l/T$. Second we parametrize the temperature dependence of the annihilation cross section as

$$\langle \sigma v_{\rm rel} \rangle = \sigma_0 x^{-n} \tag{10}$$

where $n = 0$ corresponds to s-wave annihilation, $n = 1$ to p-wave annihilation, etc. At early times n_l is accurately approximated by $n_l^{\rm eq}$, but as the temperature drops below the mass m_l, $n_l^{\rm eq}$ drops exponentially until a point denominated "freeze-out" is reached where the reaction rate is not fast enough to maintain equilibrium. From this point on, the $n_l^{\rm eq}$ term in Eq. (9) can be neglected and the remaining equation is easily integrated. Thus the solution of (9) is given by solving in two regimes and matching those solutions at the freeze-out. The value of the freeze-out point x_f is obtained by imposing the equality between the interaction rate $\Gamma = n_l \sigma v_{\rm rel}$ and the expansion rate H, and it is given by the numerical solution of the following equation:

$$x_f + (n + \tfrac{1}{2}) \ln x_f = \ln[0.038(n+1)(g/g_*^{1/2}) m_{\rm Pl} m_l \sigma_0], \tag{11}$$

where the Planck mass is $m_{\rm Pl} = 1.22 \times 10^{19}$ GeV and g_* is the number of effectively relativistic degrees of freedom at the time of freeze-out. The present mass density of the relic particles is expressed as

$$\Omega_l h^2 = (n+1) \frac{x_f^{n+1}}{g_*^{1/2}} \frac{0.034 \text{ pb}}{\sigma_0}. \tag{12}$$

In our model, we are dealing with a cold relic; therefore in the early universe, just before the decoupling, thermal equilibrium is maintained via LNP annihilations into fermions. There are two possible processes: Z boson exchange and Higgs boson exchange, both p-wave. Cross sections for these processes and their thermal averages are given in Appendix A. In the following discussion, we fix the values of Yukawa couplings and analyze the model as a function of (μ, M) for each case. The limit of small Yukawa couplings λ, λ^c is not interesting, since in this case the LNP coincides approximately with the singlet, and the only way to produce all the dark matter observed is with the LNP mass near the Z pole or the Higgs pole. If $\lambda^c = \lambda$ the model possesses a $SU(2)_L \times SU(2)_R$ symmetry broken to $SU(2)_V$ by the Higgs vacuum expectation value, and the coupling with the Z boson is suppressed. Also in this case the only way to produce all the dark matter is near the Higgs pole.

We consider for the complete analysis two limiting cases: almost equal Yukawa couplings (symmetric case or, more properly, nearly symmetric) and when one of them is vanishingly small (asymmetric case). To be consistent with negative searches from LEP, we assume $m_l \geq 45$ GeV and $M \geq 100$ GeV. The cases which we discuss are (the reason for doing so is explained in Sec. V)

(i) Symmetric case: $\alpha = 1.0$ and $\beta = 0.1$,
(ii) Asymmetric case I: $\alpha = 0.5$ and $\beta = 0.5$,
(iii) Asymmetric case II: $\alpha = 0.65$ and $\beta = 0.65$.

Before proceeding, we must say something about the Higgs boson mass, since the annihilation cross section for Higgs exchange depends on it, and we have to choose its value carefully. We will see in Sec. V that in the symmetric case the corrections to the electroweak parameter T are negligible; then the indirect upper limit on the Higgs mass valid in the standard model ($m_h \lesssim 166$ GeV at 95% CL [11]) remains unchanged. On the contrary, in the asymmetric cases T is strongly affected by the new particles, so the upper limit is raised. We choose the reference values as follows,

(i) Symmetric case: $m_h = 120$ GeV,
(ii) Asymmetric cases I and II: $m_h = 300$ GeV.

We plot our results in the (μ, M) plane in Fig. 1. In the symmetric case only the relative sign of μ and M is physical, and our convention is $M > 0$. In the asymmetric case both signs are unphysical; then we choose $\mu > 0$ and $M > 0$. We identify the parameter space region for which $45 \text{ GeV} \leq m_l \leq 75$ GeV, and inside it we shade the area for which $0.089 \leq \Omega_l h^2 \leq 0.122$ (corresponding to the 95% CL region from WMAP [2]). In all the cases the dark matter abundance can be accounted for by our LNP.

Another check must be done: neutral particles could have been produced at LEP2,

$$e^+ e^- \rightarrow \chi_l \chi_{\rm nl} \tag{13}$$

where the index nl stands for "next to lightest." Given the assumed symmetry (3) the only allowed decay for $\chi_{\rm nl}$ is

$$\chi_{\rm nl} \rightarrow \chi_l f \bar{f} \tag{14}$$

where f indicates a generic fermion and $\bar{f}$ the corresponding antifermion. Since no such event was seen, this may constrain the model. We have checked that it has not been kinematically allowed at LEP2, since the next to lightest

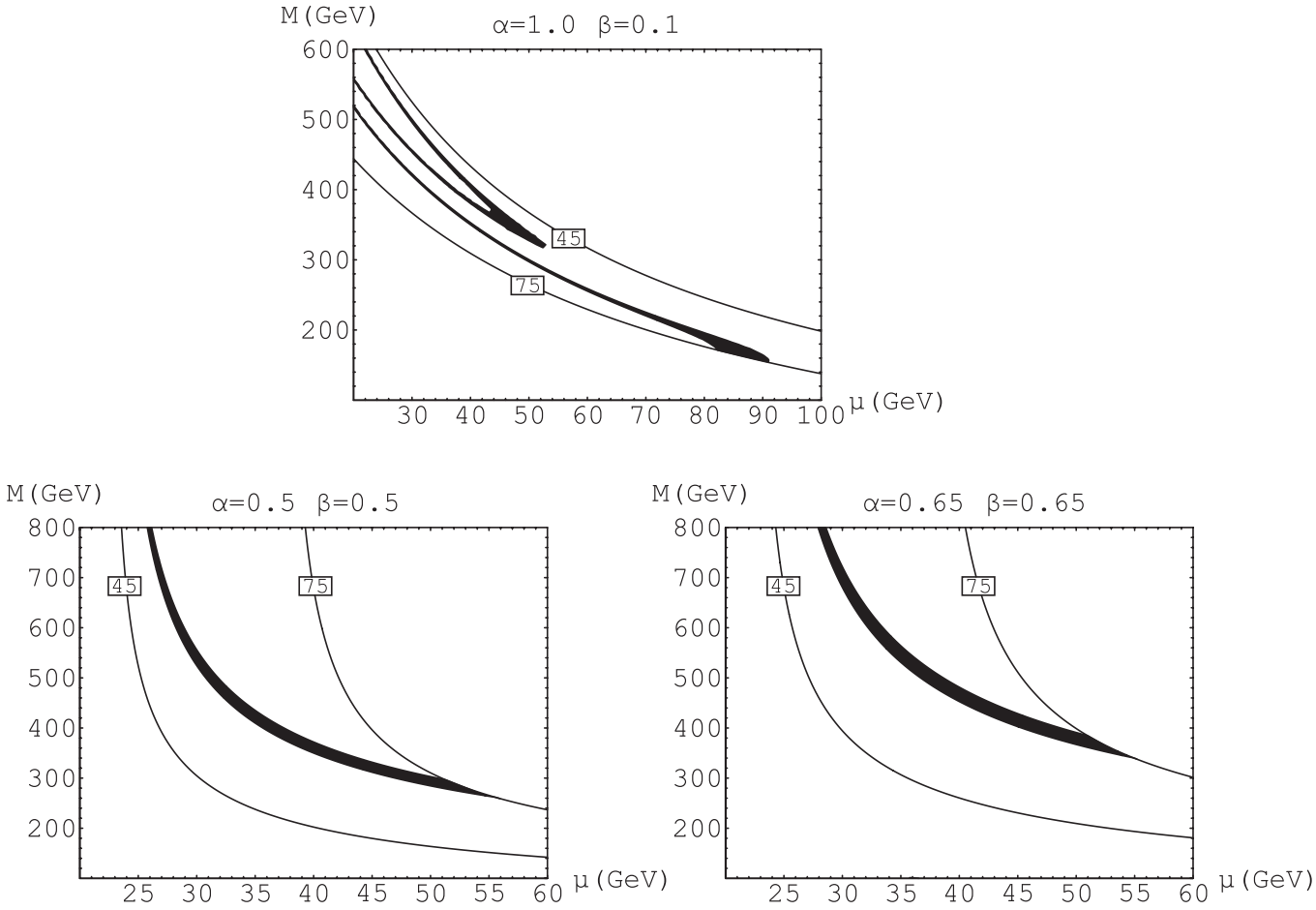

FIG. 1. LNP relic abundance. Contours for $m_l = 45, 75$ GeV are denoted by the solid lines; shaded regions correspond to $0.089 \leq \Omega_l h^2 \leq 0.122$ (WMAP 95% CL region).

particle mass is always above 200 GeV in the parameter space region of interest.

IV. DIRECT DETECTION

Dark matter particles of the Milky Way might be detectable as they pass through detectors in laboratories on Earth. The very low cross section of WIMPs on ordinary material makes these interactions quite rare, but recent experiments have made progress. The direct detection experiments can measure and distinguish from background the tiny energy deposited by elastic scattering of a WIMP off a target nucleus. The current experimental results set limits on WIMP-nucleon cross sections, and we compare LNP-nucleon cross sections given in Appendix B with these limits. Dark matter particles in the Milky Way halo presumably have a mean speed $\langle v \rangle \simeq 300\ \mathrm{km\,s^{-1}} = 10^{-3}$ c; therefore the process can be treated in the nonrelativistic limit.

The nucleon coupling of a slow-moving Majorana fermion is characterized by two terms: spin-dependent (axial-vector) and spin-independent (scalar) terms. We consider these two contributions separately.

The spin-dependent cross section for LNP-nucleus elastic scattering is given by (B5). For a proton target $\Lambda^2 J(J+1) \simeq 1$ and the cross section is

$$\sigma_Z(LN \to LN) = 3.5(V_{1l}V_{2l})^2 \times 10^{-1}\ \mathrm{pb} \qquad (15)$$

[for the definition of V see (8)]. The cross section (15) for the three cases discussed above is always 2–3 orders of magnitude below current limits [12].

The spin-independent cross section is given by (B7). It depends sensibly on the Higgs mass, so it is different between symmetric and asymmetric cases. For scattering from a proton,

$$\sigma_h(LN \to LN) = 2.75\xi^2 \times 10^{-6}\ \mathrm{pb}\left(\frac{120\ \mathrm{GeV}}{m_h}\right)^4 = 7.04\xi^2 \times 10^{-8}\ \mathrm{pb}\left(\frac{300\ \mathrm{GeV}}{m_h}\right)^4 \qquad (16)$$

where $\xi = V_{3l}(\alpha V_{2l} + \beta V_{1l})$. For the reason explained in Sec. V, we take the former reference value in the symmetric case and the latter in the asymmetric cases. The cross section (16) for the symmetric case is plotted in Fig. 2 in units of 10^{-7} pb. It is about 1 order of magnitude above the

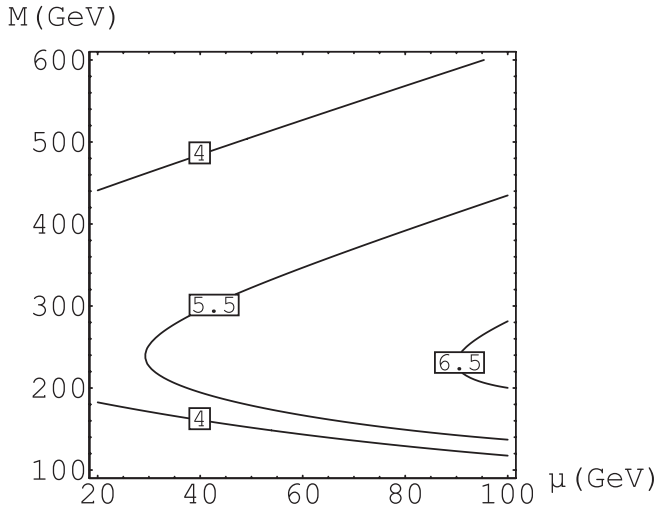

FIG. 2. Spin-independent cross section: symmetric case (in units of 10^{-7} pb).

experimental limits [13]. In the asymmetric cases, instead, the spin-independent cross section is always 1–2 orders of magnitude below current limits, but within the sensitivity of experiments currently under study [14].

V. HIGGS BOSON PHYSICS

In this section we analyze the effects on Higgs boson physics induced by the new particles. In the first subsection we compute the contributions to the electroweak observables from their virtual exchanges, and we will see that the upper limit on the Higgs mass is significantly affected. In the second subsection we analyze the new available decay channels to Higgs boson decays and compute the relevant branching ratios.

A. Electroweak precision analysis

The interaction Lagrangian of the new particles with the gauge bosons is

$$\begin{aligned}\Delta\mathcal{L}|_{\text{int}} = &-V_{1i}\frac{g}{2}W_\mu^+\bar{\psi}\gamma^\mu\chi_i + \text{H.c.} + V_{2i}\frac{g}{2}W_\mu^+\bar{\psi}\gamma^\mu\gamma^5\chi_i \\ &+ \text{H.c.} + \frac{g}{2}W_\mu^3\Big[\bar{\psi}\gamma^\mu\psi + \frac{1}{2}(V_{1i}V_{2j} + V_{2i}V_{1j}) \\ &\times \bar{\chi}_i\gamma^\mu\gamma^5\chi_j\Big] \\ &+ \frac{g'}{2}B_\mu\Big[\bar{\psi}\gamma^\mu\psi - \frac{1}{2}(V_{1i}V_{2j} + V_{2i}V_{1j}) \\ &\times \bar{\chi}_i\gamma^\mu\gamma^5\chi_j\Big] \end{aligned} \tag{17}$$

where sums under repeated indices are understood. The new particle contributions to T and S are, respectively,

$$\begin{aligned}T = &\sum_{i=1}^{3}[(V_{1i})^2\tilde{A}(M, m_i) + (V_{2i})^2\tilde{A}(M, -m_i)] \\ &- \frac{1}{2}\sum_{i,j=1}^{3}(V_{1i}V_{2j} + V_{2i}V_{1j})^2\tilde{A}(m_i, -m_j),\end{aligned} \tag{18}$$

$$S = \frac{1}{2}\sum_{i,j=1}^{3}(V_{1i}V_{2j} + V_{2i}V_{1j})^2\tilde{F}(m_i, -m_j) - \tilde{F}(\mu, \mu). \tag{19}$$

The functions $\tilde{F}$ and $\tilde{A}$ are defined in Appendix C.

We now have all the ingredients to perform the analysis. We have verified that in the symmetric case the contribution to T is negligible, as required by the custodial symmetry mentioned in Sec. III, whereas in the asymmetric cases S is not significantly affected. The experimental contours in the (S, T) plane are shown in Fig. 3 and our results for the significant cases are shown in Fig. 4.

In the symmetric case ΔT is irrelevant and ΔS is inside the experimental ellipse for almost all the region that provides the entire dark matter abundance; if we raise the value of Yukawa couplings, then ΔS goes rapidly outside the ellipse, so we restrict ourselves just to this symmetric case and we do not consider higher values of α. Looking at Fig. 3 one can immediately see how a heavy Higgs can be allowed by electroweak precision test (EWPT): the only thing that we need is new physics producing a positive ΔT and a not too large ΔS. To raise the Higgs mass up to 500 GeV the needed compensation is $\Delta T \approx 0.2$ [8]. The asymmetric case is perfectly suited to this purpose: it gives

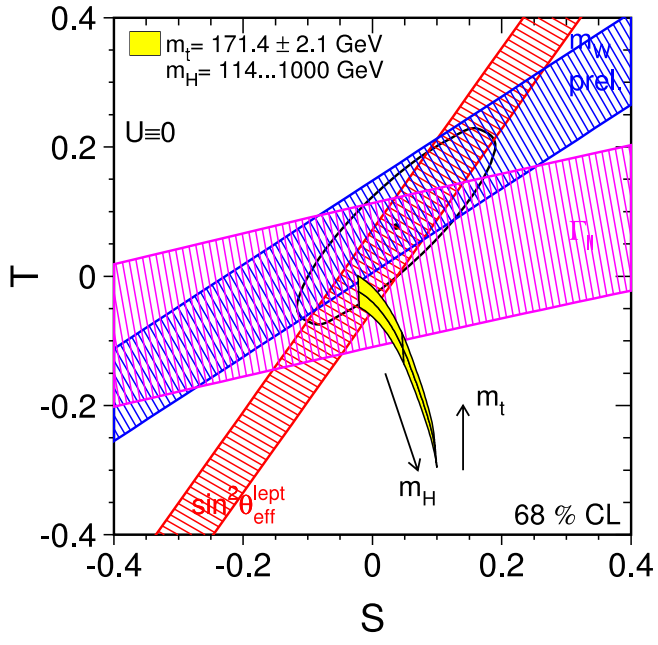

FIG. 3 (color online). Region of the (S, T) plane allowed by EWPT at 68% CL and dependence of S and T on the Higgs mass. The thin black line marks $m_h = 400$ GeV (from [22]).

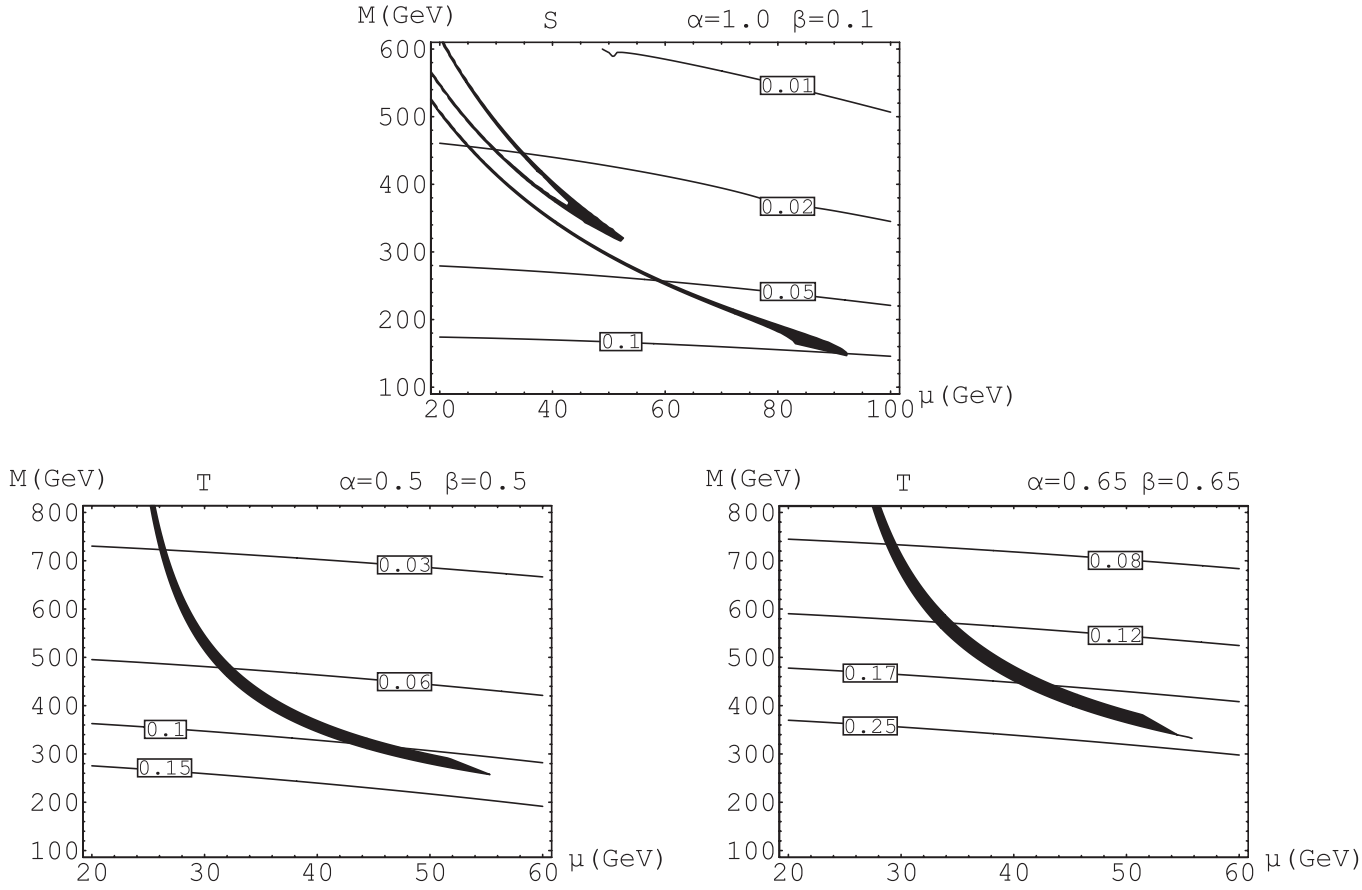

FIG. 4. S in the symmetric case and T in the asymmetric cases. The shaded regions are such that $0.089 \leq \Omega h^2 \leq 0.122$.

unimportant ΔS and a positive ΔT as desired. We first studied the case of Yukawa coupling λ^c equal to 1; then we raised its value until we reached $\Delta T \approx 0.2$, and this corresponds to $\lambda^c = 1.3$ or equivalently $\alpha = 0.65$. All the values of λ and λ^c that we consider are consistent with a Landau pole for the Yukawa coupling above the unification scale. When the Higgs boson mass is raised, however, the Higgs quartic coupling is very likely to have a Landau pole below the unification scale.

B. Higgs boson decays

Another important effect on the Higgs boson physics is the increase of its total width. In the parameter space region of interest to us, the only new available decay channel is $h \rightarrow \chi_l \chi_l$, since the decays into other new particles are kinematically forbidden. The partial width for such decay results in

$$\Gamma_{\chi\chi} = \xi^2 \frac{m_h}{2\pi}\left(1 - \frac{4m^2}{m_h^2}\right)^{3/2} \tag{20}$$

where the parameter ξ is defined in (A3). The Higgs total width predicted by the standard model Γ_h^{SM} is known as a function of m_h [15]. We consider four values for the Higgs mass, and the correspondent SM widths are reported here:

m_h (GeV)	Γ_h^{SM} (GeV)
120	3.65×10^{-3}
150	1.67×10^{-2}
200	1.425
300	8.50

The partial width $\Gamma_{\chi\chi}$ for decay into two LNPs is given by (20), and thus we can compute the branching ratio

$$\mathrm{BR}\,(h \rightarrow \chi\chi) = \frac{\Gamma_{\chi\chi}}{\Gamma_h^{\mathrm{SM}} + \Gamma_{\chi\chi}}. \tag{21}$$

For $m_h = 120$ GeV we compute the branching ratio in the symmetric case, whereas for higher masses we make the calculation for both the asymmetric cases. As seen from Fig. 1 in both the asymmetric cases the only free parameter is M, since if we impose $\Omega_l h^2 = 0.105$ the value of μ is automatically fixed. This is not true for the symmetric case, where for each M there are up to three values of μ. The branching ratios are plotted as a function of M. In the asymmetric cases it is the only free parameter. In the symmetric case, we consider the line of Fig. 1 corresponding to the lower value of the LNP mass. For the line corresponding to higher values of the LNP mass, the decay is kinematically forbidden. For the line in the middle, even

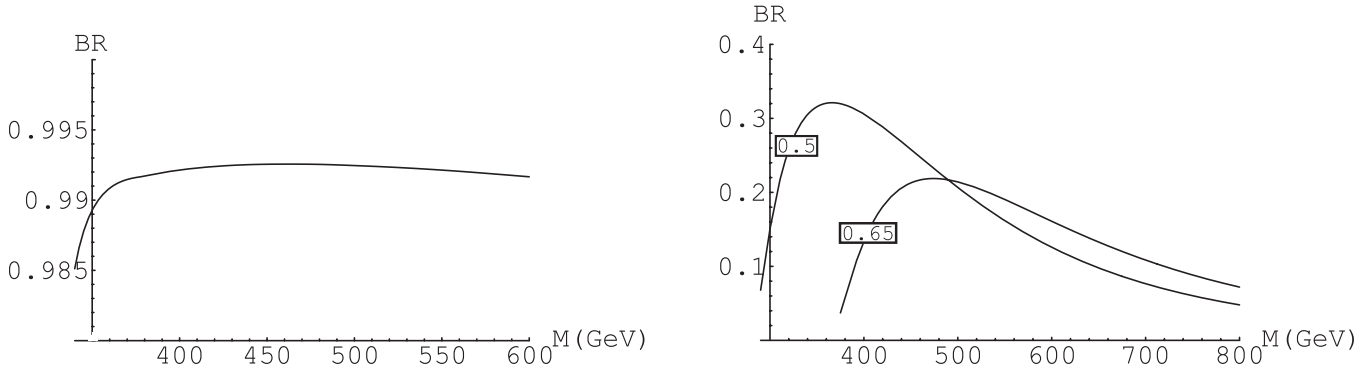

FIG. 5. Branching ratio as a function of M for $m_h = 120$ GeV (left panel) and for $m_h = 150$ GeV (right panel). Labels indicate the value of α.

small pole effects might modify the branching ratios considerably, because we are in a region where the phase space is nearly saturated.

The branching ratios for $m_h = 120$ GeV and for $m_h = 150$ GeV are plotted in Fig. 5. In the symmetric case this channel dominates the total width. For higher values of the Higgs boson mass, the branching ratios decrease, as a consequence of the standard model width increasing faster than the partial width for decay into two LNPs. For $m_h = 200$ GeV they are always below 4%, while for higher values of the Higgs mass they are even smaller.

VI. ELECTRIC DIPOLE MOMENT

We have taken the parameters $(\lambda, \lambda^c, M, \mu)$ to be real until now. We now explore the possibility of a CP violating phase. This phase could be present only in the symmetric case, since if one of the Yukawa couplings vanishes (as in the asymmetric case) all the parameters can be made real by a field redefinition. In the general case we can redefine fields so that $(\lambda, \lambda^c, \mu)$ are real, leaving a residual phase on the parameter M. The mass matrix M_N found in (6) becomes

$$M_N = \begin{pmatrix} Me^{i\theta} & 0 & -\sqrt{2}\beta v \\ 0 & -Me^{i\theta} & -\sqrt{2}\alpha v \\ -\sqrt{2}\beta v & -\sqrt{2}\alpha v & -2\mu \end{pmatrix}. \tag{22}$$

The phase θ induces an electron EDM at two loops; the dominant diagram responsible for this is generated by charged and neutral particles and is shown in Fig. 6 [7].

The induced EDM moment is given by

$$\frac{d_f^W}{e} = \pm \frac{\alpha^2 m_f}{8\pi^2 s_W^4 m_W^2} \sum_{i=1}^{3} \frac{m_{\chi_i} M}{m_W^2} \mathrm{Im}(O_i^L O_i^{R*}) \mathcal{G}(r_i^0, r^\pm) \tag{23}$$

where

$$\mathcal{G}(r_i^0, r^\pm) = \int_0^{+\infty} dz \int_0^1 \frac{d\gamma}{\gamma} \int_0^1 dy \frac{yz(y + z/2)}{(z + y)^3 (z + K_i)}$$
$$= \int_0^1 \frac{d\gamma}{\gamma} \int_0^1 dy y \left[\frac{(y - 3K_i)y + 2(K_i + y)y}{4y(K_i - y)^2} + \frac{K_i(K_i - 2y)}{2(K_i - 2y)^3} \ln \frac{K_i}{y} \right] \tag{24}$$

and

$$K_i = \frac{r_i^0}{1 - \gamma} + \frac{r^\pm}{\gamma}, \qquad r^\pm \equiv \frac{M^2}{m_W^2}, \qquad r_i^0 \equiv \frac{m_{\chi_i}^2}{m_W^2},$$
$$O_i^R = \sqrt{2} V_{2i}^* \exp(-i\theta), \qquad O_i^L = -N_{3i}. \tag{25}$$

The matrix V diagonalizes the mass matrix and is such that $V^T M_N V = \mathrm{diag}(m_1, m_2, m_3)$ with real and positive diagonal elements. The sign on the right-hand side of Eq. (23) corresponds to the fermion f with weak isospin $\pm 1/2$, and f' is its electroweak partner.

The experimental limit on the electron electric dipole moment at the 95% CL level is [16]

$$|d_e| < 1.7 \times 10^{-27} \text{ e cm}. \tag{26}$$

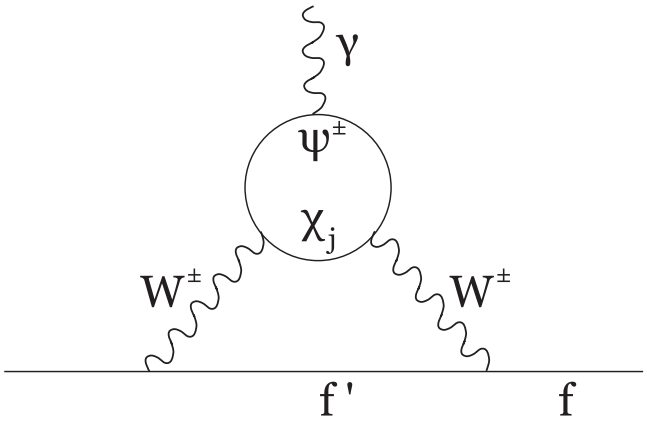

FIG. 6. Two-loop contribution to the electric dipole moment of a fermion f.

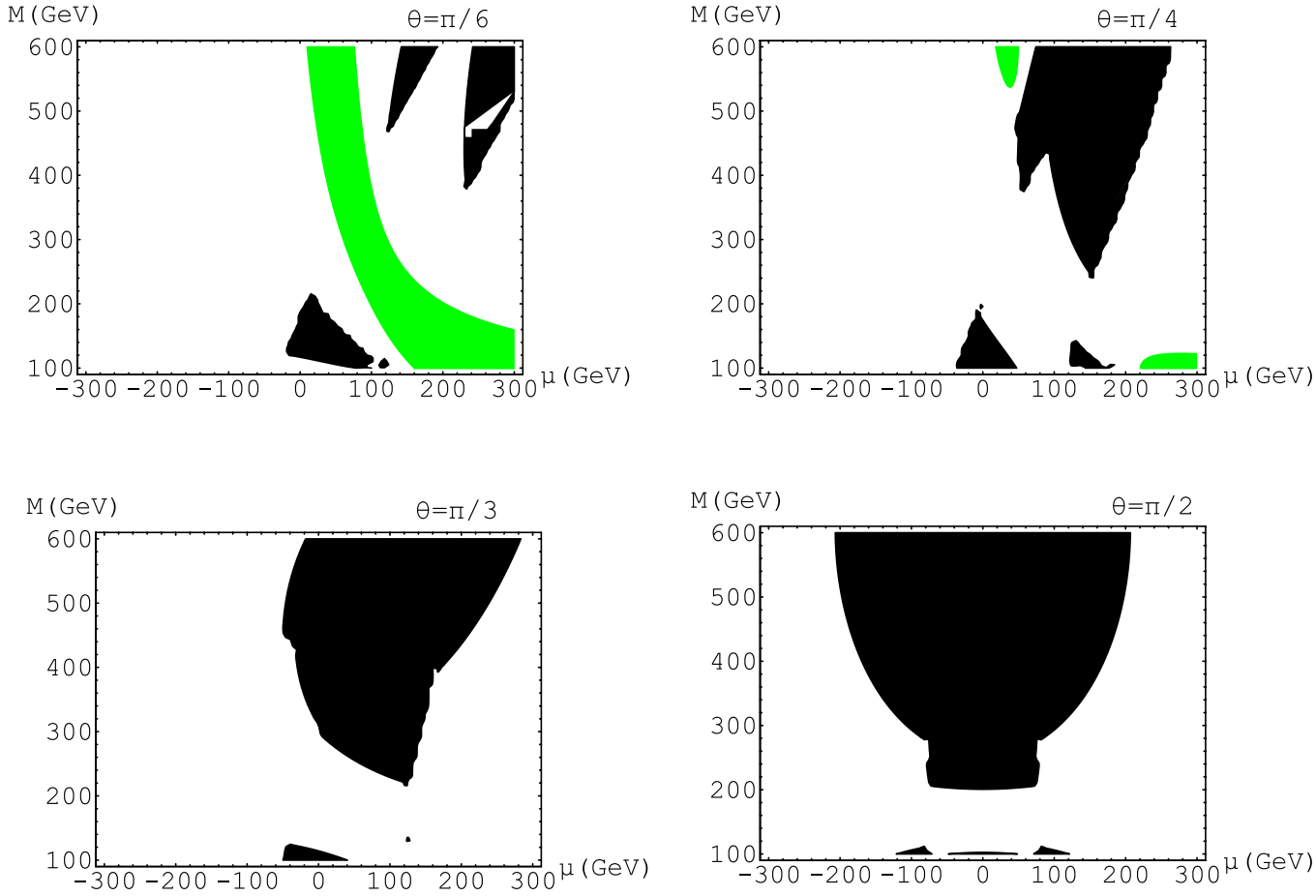

FIG. 7 (color online). Induced electron EDM for $\theta = \frac{\pi}{6}, \frac{\pi}{4}, \frac{\pi}{3}, \frac{\pi}{2}$. Green (lightest) regions are such that $m_l \leq 75$ GeV; black shading indicates regions where the induced EDM is above the experimental limit.

We consider four different values of the phase, namely, $\theta = \pi/6,\ \pi/4,\ \pi/3,\ \pi/2$, and we shade in the usual (μ, M) plane the regions where the induced EDM is above such limit. We also identify in that plane the region where the LNP mass is below 75 GeV, since this is the case in which we are interested. We also restrict ourselves to charged particle mass M below 600 GeV, as in the plot shown in Fig. 1. The plots are shown in Fig. 7. The first result is that, for $M < 600$ GeV, we can have a LPN mass below 75 GeV only for small phases; otherwise the imaginary part that was not present before would require a cancellation in the mass matrix obtainable only for a higher value of M. Regarding the induced EDM, there are regions where it is above the experimental limit, but never inside regions such that $m_l < 75$ GeV. On the contrary, for $m_l < 75$ GeV, the induced EDM is always below the limit (26). It could, however, be accessible to next-generation experiments [17,18].

VII. CONCLUSIONS

In the last few decades it has been realized that the ordinary matter which we have been studying until now constitutes only about 5% of the total universe energy density. Evidence for nonluminous gravitating mass abounds on all the scales, from galactic to global ones of hundreds of Megaparsec. The measurements of the light element abundances and of the fluctuations in the cosmic microwave background show that a significant part of the dark matter must be nonbaryonic. The standard model of particle physics does not contain such a component. Another missing opportunity for the standard model is that gauge coupling unification does not occur at high energy. In this work we have discussed a minimal extension of the standard model, which can explain all the observed dark matter abundance and improve the gauge coupling unification, focusing on the parameter space region for which the LNP mass is below $m_W \approx 80$ GeV. For such a region the effects on the Higgs boson physics are worth consideration.

We have considered two limiting cases: almost equal Yukawa couplings (symmetric) and one of them vanishing (asymmetric). In both cases all the observed dark matter abundance could be explained by the LNP. We have computed also the full spectra of the model for all the cases, and they are consistent with negative searches from LEP2. The

spin-independent direct detection cross section is above the current limits only for the symmetric case. In the asymmetric case it is well below these limits, as the spin-dependent cross sections for both cases. However, they are all within the sensitivity of experiments currently under study.

The new particles might have both direct and indirect effects on the Higgs boson physics. We have analyzed these effects and found that they are very different for each case. In the symmetric case the contribution to the electroweak observables is small, but the Higgs decays in LNP pairs dominate the total width. This might hide the Higgs boson at the CERN Large Hadron Collider. On the contrary, in the asymmetric case the contribution to the EWPT is important, and the indirect limit on the Higgs mass valid in the standard model can be raised. Finally, we have considered a *CP* violating phase for the Dirac mass of the charge particle, giving rise to an electron electric dipole moment. We have verified that, if we keep the LNP mass below 75 GeV, the induced electric dipole moment is always below the current experimental limit, but perhaps accessible at the next-generation experiments.

ACKNOWLEDGMENTS

I would like to thank Riccardo Barbieri for his constant presence and guidance, without which this work would have never been completed, and for the careful reading of the manuscript. I am grateful to Vyacheslav S. Rychkov for some precious suggestions concerning numerical computation and to Alessandro Strumia for useful discussions concerning direct detection experimental limits.

APPENDIX A: ANNIHILATION CROSS SECTIONS

1. *s*-channel *Z* exchange

The LNP has a coupling with the Z boson given by

$$\frac{g}{2c_W}(V_{1l}V_{2l})Z_\mu \bar{\psi}_l \gamma^\mu \gamma^5 \psi_l. \tag{A1}$$

The cross section for the process $\chi_l\chi_l \to Z^* \to f\bar{f}$ for nonrelativistic LNPs and in the limit of massless final products is

$$\sigma_Z v_{\rm rel} = \Sigma(g_V^2 + g_A^2)\frac{g^4(V_{1l}V_{2l})^2}{24\pi c_W^4}\frac{m^2}{(4m^2 - m_Z^2)^2}v_{\rm rel}^2 \tag{A2}$$

where the sum runs over all the standard model fermions except for the top quark.

2. *s*-channel *h* exchange

The coupling between the LNP and the Higgs boson is

$$\xi\bar{\psi}_l\psi_l h, \qquad \xi \equiv V_{3l}(\alpha V_{2l} + \beta V_{1l}). \tag{A3}$$

The cross section for the process $\chi_l\chi_l \to h^* \to f\bar{f}$, kinematically identical to the previous one, is

$$\sigma_h v_{\rm rel} = \frac{\xi^2}{4\pi}\frac{m^2 m_b^2}{v^2(4m^2 - m_h^2)^2}v_{\rm rel}^2 \tag{A4}$$

where m_b is the mass of the b quark (the process with $b\bar{b}$ in the final state is dominant, since $\sigma_h \propto m_f^2$).

3. Thermally averaged cross sections

To compute the thermally averaged cross section it is useful to observe that in both cases

$$\sigma_j v_{\rm rel} = b_j v_{\rm rel}^2 \tag{A5}$$

where $j = Z$, h, respectively, for Z exchange and for h exchange. Performing the thermal average we obtain

$$\langle \sigma_j v_{\rm rel}\rangle = 6\frac{b_j}{x}, \tag{A6}$$

so in our case the value of σ_0 is given by

$$\sigma_0 = 6(b_Z + b_h). \tag{A7}$$

APPENDIX B: LNP-NUCLEUS ELASTIC CROSS SECTIONS

1. Spin-independent cross section

The elastic scattering process is $\chi_l\mathcal{N} \to Z^* \to \chi_l\mathcal{N}$ where $\mathcal{N}$ is a generic nucleus. The vertex between quarks and the Higgs boson is given by the standard model Lagrangian and results in

$$\frac{g}{c_W}Z^\mu J^0_\mu. \tag{B1}$$

The weak neutral current of the quarks J^0_μ is of the form $\sum_q \bar{q}\,\gamma^\mu(c_V^q - c_A^q\gamma^5)q$, where the parameters c_V^q and c_A^q are known as a function of the Weinberg angle only. We have two different contributions to the amplitude: the quark vector current and the quark axial-vector current. We can neglect the first contribute for nonrelativistic LNPs. The vector-axial contribution is described by the effective Lagrangian

$$\mathcal{L}_{\rm axial} = (V_{1l}V_{2l})\bar{\Psi}_L\gamma^\mu\gamma^5\Psi_L\sum_q \zeta_q\bar{q}\gamma_\mu\gamma^5 q \tag{B2}$$

where we define $\zeta_q \equiv 2\sqrt{2}G_F c_A^q$.

We introduce the parameters

$$a_p = \sum_q \frac{\zeta_q}{\sqrt{2}G_F}\Delta q^{(p)} = \sum_q 2c_A^q \Delta q^{(p)},$$
$$a_n = \sum_q \frac{\zeta_q}{\sqrt{2}G_F}\Delta q^{(n)} = \sum_q 2c_A^q \Delta q^{(n)}, \tag{B3}$$

$$\Lambda = \frac{a_p\langle S_p\rangle + a_n\langle S_n\rangle}{J}. \tag{B4}$$

The quantity J is the total angular momentum of the nucleus; $\langle S_p\rangle$ is the expectation value of the spin content of the proton group in the nucleus, and similarly for $\langle S_n\rangle$. The total cross section is [19]

$$\sigma_Z(LN \to LN) = \frac{32}{\pi}(V_{1l}V_{2l})^2 G_F^2 m_r^2 \Lambda^2 J(J+1) \tag{B5}$$

where m_r is the reduced mass of the system LNP nucleus.

2. Spin-independent cross section

The elastic scattering process is $\chi_l\mathcal{N} \to h^* \to \chi_l\mathcal{N}$. The nucleonic matrix element can be parametrized by [20]

$$\langle N|\sum_q m_q \bar{q}q|N\rangle = f m_N \langle N|N\rangle, \qquad f \simeq 0.3, \tag{B6}$$

and finally the spin-independent cross section results in

$$\sigma_h(LN \to LN) = \frac{2\xi^2 f^2}{\pi}\frac{m_r^2 m_N^2}{m_h^4 v^2} \tag{B7}$$

where m_r is the reduced mass of the system LNP nucleus.

APPENDIX C: ELECTROWEAK PRECISION TEST

As is well known, new physics effects to the EWPT are conveniently represented by the parameters T and S, defined by

$$T = \frac{\Pi_{33}(0) - \Pi_{WW}(0)}{\alpha_{em} m_W^2}, \qquad S = \frac{4 s_W c_W}{\alpha_{em}}\Pi'_{30}(0) \tag{C1}$$

in terms of the vacuum polarization amplitudes

$$i\Pi_{ij}^{\mu\nu}(q) = \eta^{\mu\nu}\Pi_{ij}(q^2) + q^\mu q^\nu \text{ terms} \tag{C2}$$

with $i, j = 3, 0, W$ for W_3^μ, B^μ, W^μ, respectively.

Expressions for the vacuum polarization amplitudes produced by fermions coupled to a generic gauge boson are known [21]. For a fermion loop with internal masses m_1 and m_2 and a vector coupling $V_\mu \bar{\Psi}_1 \gamma^\mu \Psi_2$, it is

$$\Pi(0) = \frac{1}{16\pi^2}\left[(m_1 - m_2)^2 \ln\frac{\Lambda^4}{m_1^2 m_2^2} - 2m_1 m_2 + \frac{2m_1 m_2(m_1^2 + m_2^2) - m_1^4 - m_2^4}{m_1^2 - m_2^2}\ln\frac{m_1^2}{m_2^2}\right], \tag{C3}$$

$$\Pi'(0) = \frac{1}{24\pi^2}\left[-\ln\frac{\Lambda^4}{m_1^2 m_2^2} - \frac{m_1 m_2(3m_1^2 - 4m_1 m_2 + 3m_2^2)}{(m_1^2 - m_2^2)^2} + \frac{m_1^6 + m_2^6 - 3m_1^2 m_2^2(m_1^2 + m_2^2) + 6m_1^3 m_2^3}{(m_1^2 - m_2^2)^3}\ln\frac{m_1^2}{m_2^2}\right]. \tag{C4}$$

For an axial coupling the results are obtained by letting $m_1 \to -m_1$ in the previous expressions. These results are valid for Dirac fermions; for Majorana fermions there is an extra factor of 2. Λ is a cutoff of the loop integral which disappears in the overall expressions (C1).

We define, for convenience,

$$\tilde{A}(m_1, m_2) \equiv \frac{1}{2\alpha_{em} v^2}\Pi(0), \tag{C5}$$

$$\tilde{F}(m_1, m_2) \equiv 4\pi\Pi'(0). \tag{C6}$$

[1] G. Bertone, D. Hooper, and J. Silk, Phys. Rep. **405**, 279 (2005).
[2] D. N. Spergel *et al.* (WMAP Collaboration), Astrophys. J. Suppl. Ser. **170**, 377 (2007).
[3] L. Bergstrom, Rep. Prog. Phys. **63**, 793 (2000).
[4] K. A. Olive, G. Steigman, and T. P. Walker, Phys. Rep. **333**, 389 (2000).
[5] Particle Data Group, http://pdg.lbl.gov.
[6] M. Cirelli, N. Fornengo, and A. Strumia, Nucl. Phys. **B753**, 178 (2006).
[7] R. Mahbubani and L. Senatore, Phys. Rev. D **73**, 043510 (2006).
[8] R. Barbieri, L. J. Hall, and V. S. Rychkov, Phys. Rev. D **74**, 015007 (2006).
[9] E. W. Kolb and M. S. Turner, *The Early Universe*, Frontiers in Physics (Addison-Wesley, Reading, MA, 1990).
[10] K. Griest and D. Seckel, Phys. Rev. D **43**, 3191 (1991).
[11] J. Alcaraz *et al.* (ALEPH Collaboration), arXiv:hep-ex/0612034.

[12] D. S. Akerib *et al.* (CDMS Collaboration), Phys. Rev. D **73**, 011102 (2006).
[13] J. Angle *et al.* (XENON Collaboration), arXiv:0706.0039.
[14] P. L. Brink *et al.* (CDMS-II Collaboration), arXiv:astro-ph/0503583.
[15] A. Djouadi, arXiv:hep-ph/0503172.
[16] B. C. Regan, E. D. Commins, C. J. Schmidt, and D. DeMille, Phys. Rev. Lett. **88**, 071805 (2002).
[17] Y. K. Semertzidis, Nucl. Phys. B, Proc. Suppl. **131**, 244 (2004).
[18] D. Kawall, F. Bay, S. Bickman, Y. Jiang, and D. DeMille, AIP Conf. Proc. **698**, 192 (2004).
[19] G. Jungman, M. Kamionkowski, and K. Griest, Phys. Rep. **267**, 195 (1996).
[20] R. Barbieri, M. Frigeni, and G. F. Giudice, Nucl. Phys. **B313**, 725 (1989).
[21] R. Barbieri, L. J. Hall, Y. Nomura, and V. S. Rychkov, Phys. Rev. D **75**, 035007 (2007).
[22] http://lepwwg.web.cern.ch/LEPEWWG/plots/summer2006/s06 stu contours.eps.